

Journal of Materials Chemistry B

Accepted Manuscript



This is an *Accepted Manuscript*, which has been through the Royal Society of Chemistry peer review process and has been accepted for publication.

Accepted Manuscripts are published online shortly after acceptance, before technical editing, formatting and proof reading. Using this free service, authors can make their results available to the community, in citable form, before we publish the edited article. We will replace this *Accepted Manuscript* with the edited and formatted *Advance Article* as soon as it is available.

You can find more information about *Accepted Manuscripts* in the [Information for Authors](#).

Please note that technical editing may introduce minor changes to the text and/or graphics, which may alter content. The journal's standard [Terms & Conditions](#) and the [Ethical guidelines](#) still apply. In no event shall the Royal Society of Chemistry be held responsible for any errors or omissions in this *Accepted Manuscript* or any consequences arising from the use of any information it contains.

Glypican-3 antibody functionalized prussian blue nanoparticles for targeted MR imaging and photothermal therapy of hepatocellular carcinoma

Cite this: DOI: 10.1039/x0xx00000x

Received xxthxxxxxx 20xx,
Accepted xxthxxxxxx 20xx

DOI: 10.1039/x0xx00000x

www.rsc.org/MaterialsB

Zhenglin Li ^{#,1,2}, Yongyi Zeng ^{#,1,2,3}, Da Zhang ^{1,2}, Ming Wu ^{1,2}, Lingjie Wu ^{1,2}, Aimin Huang ^{2,4}, Huanghao Yang ⁵, Xiaolong Liu ^{*,1,2} and Jingfeng Liu ^{*,1,2,3}

MRI-guided photo-thermal therapy is becoming a more widely accepted minimally invasive technique. In this study, glypican-3 monoclonal antibody functionalized prussian blue nanoparticles (antiGPC3-PBNPs) were developed as a novel theranostic agent for the targeted MR imaging and photo-thermal therapy of hepatocellular carcinoma. The physical properties of the antiGPC3-PBNPs were characterized by SEM, TEM and Vis-NIR absorption spectra, which showed that the developed nanoprobe formed well defined nanocubes with an average diameter of 21 nm. The significantly increased targeting cellular uptake efficiency in HepG2 cells *via* receptor-mediated endocytosis was confirmed by confocal fluorescence microscopy and ICP-MS. Furthermore, the high photothermal cytotoxicity, excellent MR imaging contrast enhancement ability and biocompatibility of the developed nanoprobe were also confirmed. Hence, the developed antiGPC3-PBNPs could be used as a promising nanoprobe for targeted MRI diagnosis and efficient photo-thermal therapy for hepatocellular carcinoma.

Introduction

Hepatocellular carcinoma (HCC), a highly lethal disease which usually occurs in patients with chronic parenchymal liver diseases such as chronic infection with hepatitis B or C virus or cirrhosis¹, is the fifth most prevalent malignancy worldwide and the third leading cause of cancer-related deaths, especially with 50% of cases occurring in China^{2, 3}. Up to date, the incidence of HCC is still increasing^{4, 5}, but the results of current primary curative treatments such as surgical resection, ablative therapies and liver transplantation are still unsatisfactory. One of the major obstacles is the high frequency of tumor recurrence^{6, 7}. However, the 5-year survival rates of HCC can be achieved up to 75% by the current treatments when HCC is detected at an early stage⁸⁻¹⁰. Nevertheless, the symptoms of HCC only appear in the advanced stage and early diagnosis is still difficult to achieve so far.

Currently, image-guided laser ablation, a minimally invasive technique, can be used as a therapeutic approach for cancer. Photo-thermal therapy (PTT) is a non-invasive laser-based technique to “heat” tumor cells with the help of photo-absorbers, such as Au nanorods¹¹, Au nanoshells¹², carbon nanotubes¹³, and copper chalcogenide semiconductors¹⁴ which can convert optical energy into thermal energy and then cause photo-induced heating of cancer cells without affecting surrounding healthy tissues¹⁵. Due to the minimal absorption of near-infrared (NIR, $\lambda = 700\sim 1100$ nm) light in biological tissues and the optimal penetration depth¹⁶, photo-thermal

agents which respond strongly to NIR light excitation have attracted special interest. However, the precondition of PTT treatment is to precisely identify the spatial location and size of the tumor, and ensure the photo-absorbers accumulate at the tumor site, therefore appropriate imaging modalities are necessary to monitor the treatment procedure during therapy¹⁷⁻¹⁹. Among numerous clinically available imaging modalities for detecting hepatocellular carcinoma, magnetic resonance imaging (MRI) is a non-invasive and non-ionizing imaging modality with a typical resolution of 100 μ m, as it provides exquisite 3D soft tissue details and functional information of the lesions for targeted visualization and post-procedure follow-up²⁰. Moreover, MRI can provide non-invasive thermometry as the feedback information for the PTT procedure^{19,21}. Prussian blue nanoparticle (PBNP) is a latest developed photo-thermal agent, which intrinsic NIR region absorption derived from the charge transfer transition between Fe(II) and Fe(III) in PBNPs instead of surface plasmon resonance²². Thus, the PBNPs have a better photo-thermal stability compared with Au nanoshells and Au nanorods, which were the most commonly used materials as effective hyper-thermal therapeutic agents but would diminish after a long period of laser irradiation due to the “melting effect”²³. Moreover, earlier studies have demonstrated the potential use of PBNPs as an effective MRI contrast agent^{24, 25}. However, it should be noted that great efforts are still needed to improve the ability of PBNPs for further clinical application, particularly the targeting ability for a particular tumor such as HCC.

Many HCC-targeting systems which are mostly based on the NPs modified with tissue-specific ligands (like vascular endothelial growth factor, epidermal growth factor receptor, aptamers and small molecules such as galactose) have been reported for use in HCC diagnostics and therapeutics²⁶⁻³¹. However, many of them show less specificity and capability of differentiating HCC from regenerating nodules, regardless of the etiology or stage of hepatic pathology. Recent studies have revealed that glypican-3 (GPC3), a family of heparan sulfate proteoglycans essential in regulating embryo cell growth³², is a more sensitive and more specific biomarker for detecting early stage of HCC, especially compared with alpha-fetoprotein (AFP) which is the most utilized surveillance biomarker for HCC³³. Moreover, the expression rate of GPC3 (77%) is significantly higher than the AFP in the serum (43%) and in the HCC tissue (41%), when the tumor size of HCC is smaller than 3 cm. Therefore, these auspicious attributes make GPC3 a promising early diagnostic biomarker for HCC targeting³⁴.

Herein, a multifunctional nanoprobe based on GPC3 antibody-mediated HCC-targeting prussian blue nanoparticles (antiGPC3-PBNPs) were developed as a novel theranostic agent for the targeted PTT and MR imaging of HCC treatments. The physical properties of the multifunctional nanoprobe are characterized by SEM, TEM and Vis-NIR absorption spectra. Furthermore, the *in vitro* cellular uptake, photo-thermal cytotoxicity and MR imaging of antiGPC3-PBNPs were also performed to evaluate its targeted photo-thermal ablation and imaging ability to HCC.

Materials and methods

Materials

1-(3-dimethylaminopropyl)-3-ethylcarbodiimide hydrochloride (EDC, Sigma-Aldrich), sulfo N-hydroxysuccinimide (NHS, Sigma-Aldrich), mouse anti-human monoclonal GPC3 antibodies (antiGPC3, ~150 kDa, Sigma-Aldrich), fluorescein isothiocyanate (FITC, Fanbo Biochemicals), Cell Counting Kit-8 (CCK8, Dojindo Laboratories). Unless otherwise stated, reagents such as $\text{FeCl}_3 \cdot 6\text{H}_2\text{O}$, $\text{K}_4[\text{Fe}(\text{CN})_6] \cdot 3\text{H}_2\text{O}$ and citric acid were of analytical grade and used as received. De-ionized water, with a resistivity of $18.2 \text{ M}\Omega \cdot \text{cm}$, was obtained from Milli-Q Gradient System (Millipore, Bedford, MA, USA) and used for all the experiments.

Instruments

Vis-NIR absorbance of PBNPs and antiGPC3-PBNPs in DMEM medium contained 10% fetal bovine serum were measured by using a TU-1950 Vis-NIR spectrophotometer (Beijing Perkinje General Instrument Co., China) at room temperature. The morphology and particle size of the prepared samples were characterized by Scanning Electron Microscopy (SEM, Hitachi Limited, Japan) and Transmission electron microscopy (TEM, Tecnai G20, FEI Co., USA) respectively. Energy Dispersive Spectroscopy (EDS) was used to analyze the elements in the sample of antiGPC3-PBNPs powder. The DLS experiments were performed at 25°C on a NanoZS (Malvern

Instruments, Malvern UK) with a detection angle of 173° , and a 3 mW He-Ne laser operating at a wavelength of 633 nm. The Z-Average diameter and the polydispersity index (PDI) values were obtained from analysis of the correlation functions by using Cumulants Analysis. Zeta potential measurements were performed at 25°C on the NanoZS by using the M3-PALS technology. NIR laser irradiation was performed with a continuous-wave diode NIR laser (K808D/K09F-8.00W) with a center wavelength of $808 \pm 10 \text{ nm}$ and output power of 2 W (Beijing Kaipulin Optoelectronic Technology Co., China). The temperature of the solutions was recorded by a thermocouple microprobe (STPC-510P, Xiamen Baidewo Technology Co., China). Confocal fluorescence microscopy studies of the cellular uptake efficiency were observed with a confocal laser scanning fluorescence microscopy (TCS-SP2, Leica, Germany). The iron content was determined with a XSERIES 2 inductively coupled plasma mass spectrometry (ICP-MS) (Thermo, USA).

Cell culture

HepG2 cells, are human hepatocellular carcinoma cells which express GPC3 protein confirmed by Western blotting according to the previous literature³³, and HeLa (immortalized cervical cancer) cells or normal HL-7702 hepatocytes lacking GPC3 expression were used as the negative control, respectively. These cells were cultured in Dulbecco's modified essential medium (DMEM, Gibco) supplemented with 10% fetal bovine serum (Atlanta Biologicals, Lawrenceville, GA, USA) and 1% penicillin-streptomycin (Gibco BRL, Grand Island, NY, USA) at 37°C in a 5% CO_2 atmosphere, and sub-cultivated at a ratio of 1:4 twice a week by using Trypsin-EDTA Solution.

Preparation of citrate-coated PBNPs

According to the previous literature^{22, 24, 25}, PBNPs were prepared in a simple one-step aqueous solution route using citric acid as the surface capping agent which could prevent PBNPs from aggregation and mediate the size of PBNPs. In a typical procedure, 5.4 mg of $\text{FeCl}_3 \cdot 6\text{H}_2\text{O}$ was dissolved in DI water (20.0 mL) under stirring at 60°C , followed by the addition of citric acid (98.0 mg, 0.5 mM). Then, 20.0 mL of $\text{K}_4[\text{Fe}(\text{CN})_6]$ aqueous solution (1.0 mM) which contained the same amount of citric acid was added drop-wise into the above 1.0 mM FeCl_3 aqueous solution under stirring at 60°C . During the mixing process, a clear bright blue dispersion formed immediately and the pH of this dispersion was measured to be approximately 2.8. After that, the mixture solution was under continuous stirring at 60°C for another 5 min, and then allowed to cool down to room temperature with continued stirring for another 30 min.

An equal volume of acetone was added to the above dispersion and the mixture was then centrifuged at 12500 rpm for 60 min to form the PBNPs precipitation. After removing the supernatant, the obtained precipitation was re-suspend in 20.0 mL DI water by sonication. For purification of the PBNPs, the above wash step was repeated three times and the obtained

precipitate was dried in an oven under vacuum at 50°C for 12 h to obtain the PBNPs powder.

Preparation of antiGPC3-PBNPs

A one-pot coupling method was used to couple the GPC3-associated monoclonal antibody to the PBNPs, which has been reported by previous research^{33, 35, 36}. Briefly, 1.0 mg of PBNPs powder was re-dispersed in 4.0 mL phosphate-buffered solution (pH=7.4) by sonication, and 0.2 M HCl was then titrated into the mixed solution to adjust the pH to 5.0. For activating the surfaces of the citrate-coated PBNPs prior to GPC3 antibody covalent grafting, 4.0 mg 1-(3-dimethylaminopropyl)-3-ethylcarbodiimide hydrochloride (EDC) and 8.0 mg sulfo N-hydroxysuccinimide (NHS) were added into the PBNPs solution, which was followed by reacting on a shaker for 2 hours. After that, 4.0 μ L GPC3 antibody (10.0 mg mL⁻¹) was added in, stirred slightly until fully mixed, and allowed to react with continuous mechanical oscillation for 3 hours at room temperature. Then the mixture was react at 4°C overnight. Finally, 0.2 M NaOH solution was titrated into the mixed solution to adjust the pH to 7.0. After 30 minutes, the reaction solution was centrifuged at 4°C and the obtained pellet of precipitation was re-suspended in PBS buffer (pH=7.4). After washed for another three more times, the obtained precipitate was re-dispersed in PBS at 4°C before use.

Confocal fluorescence microscopy studies of the cellular uptake efficiency

Fluorescein isothiocyanate (FITC), a typical fluorescent dye, was used to label antiGPC3-PBNPs for confocal fluorescence microscopy studies of the cellular uptake efficiency of antiGPC3-PBNPs. We prepared the FITC-labeled antiGPC3-PBNPs sample based on the previous published procedure^{37, 38}. Then, HepG2 cells, HeLa cells and normal HL-7702 hepatocytes were cultured on coverslips at a density of 1×10^4 cells per well at 37°C in a 5% CO₂ atmosphere for 24 hours. The cell culture medium was discarded and the cells were washed three times with PBS to remove dead cells, followed by incubation with 250 ppm FITC-labeled antiGPC3-PBNPs dispersions at 37°C in a humidified atmosphere containing 5% CO₂ for 2 and 4 hours, respectively. After incubation, the cells were washed with PBS buffer, and the nuclei were stained with 2.0 μ M DAPI, then the cells were fixed with 4% paraformaldehyde for 20 min. Afterwards, the coverslips were taken out and imaged with a confocal laser scanning fluorescence microscopy (CLSM) (TCS-SP2, Leica, Germany), with 488 nm laser excitation of FITC and 405 nm laser excitation of DAPI.

Quantification of antiGPC3-PBNPs uptake by ICP-MS

HepG2 cells and normal HL-7702 hepatocytes were seeded onto six-well plates with a density of 2.5×10^5 cells per well, then cultured at 37°C with 5% CO₂ for 24 hours. Afterwards, both cells were incubated with fresh medium containing gradient concentrated antiGPC3-PBNPs or PBNPs (50, 100,

250 ppm) for 4 hours at 37°C with 5% CO₂ atmosphere, respectively. Meanwhile, both cells were also incubated with a fixed concentration of 250 ppm antiGPC3-PBNPs or PBNPs dispersions for 1, 2, and 4 hours, respectively. After washed three times with PBS to remove free particles, the adherent cells were trypsinized, and collected by centrifugation for 5 minutes (1500 rpm, 20°C). The cells were then re-suspended in PBS and counted by using a hemocytometer. Thereafter, the cells with a density of 2.5×10^5 cells/200 μ L were used to calculate the iron content in all cell samples by ICP-MS. Briefly, 2.5×10^5 cells in 200 μ L PBS were lysed using a strong oxidizing mixture containing 1.0 mL 65% nitric acid and 200 μ L H₂O₂, and then heated to 120 °C for 1 hour in order to remove all organics. The remaining inorganic material was dissolved in 10.2 mL 2% dilute nitric acid medium and was analyzed by ICP-MS.

Photo-thermal heating experiments

Measurement of the photo-thermal effect of the antiGPC3-PBNPs induced by near infrared reflection (NIR) laser irradiation (808 nm, 2 W) was carried out by monitoring the temperature of 1.0 mL antiGPC3-PBNPs solution with various concentrations (0, 45.5, 90.9 ppm). Briefly, 1.0 mL antiGPC3-PBNPs dispersion was added in a quartz cuvettes (total volume of 3.0 mL), and then irradiated by an optical fiber coupled 808 nm high power diode-laser with an output of 2 W for 10 min. The temperature of the solutions was monitored by a thermo couple microprobe (Q50.5 mm) submerged in the solution where the direct irradiation of the laser on the probe was avoided. Meanwhile, 1.0 mL DI water was used as a control. Furthermore, the photo-thermal stability of antiGPC3-PBNPs dispersions (90.9 ppm) was also investigated by continuously irradiating with the 808 nm laser. In brief, the prepared antiGPC3-PBNPs dispersion was first irradiated for 10 min, followed by cooling to the initial temperature, and then another irradiation cycle was carried out.

In vitro photo-thermal ablation of HepG2 cells with antiGPC3-PBNPs

Localized photo-thermal cell toxicity of antiGPC3-PBNPs was evaluated on HepG2 cells. For qualitative analysis, HepG2 cells were seeded onto a six-well plate at a density of 5×10^5 cells per well at 37°C in a humidified atmosphere containing 5% CO₂ for 48 h. After that, the culture medium was replaced with 50 ppm antiGPC3-PBNPs solution and the cells were then exposed to NIR laser (2 W cm⁻²) for 10 min. After laser irradiation, the cells were incubated with fresh DMEM culture medium containing 10% fetal bovine serum at 37 °C for 1 hour, then washed with PBS and stained with 2.0 μ M calcein AM (calcein acetoxymethyl ester) for the visualization of live cells.

To further evaluate the cell survival rate after laser irradiation, Cell Counting Kit-8 (CCK-8) was used instead of conventional MTT (3-(4,5-dimethylthiazol-2-yl)-2,5-diphenyltetrazolium bromide) assay to study the photo-thermal cell toxicity of antiGPC3-PBNPs. In a typical experiment, HepG2 cells were

first seeded onto a 96-well plate at a density of 1×10^4 cells per well at 37°C in a 5% CO_2 atmosphere for 24 hours. Then, the cell culture medium was discarded and the cells were washed three times with PBS to remove dead cells, followed by incubation with different concentration of antiGPC3-PBNPs dispersed in DMEM medium (from 0 ppm to 20.0 ppm) at 37°C . After the incubation for 4 hours, the cells were irradiated with an NIR laser (808 nm, 2 W) for 8 min. Then, CCK-8 Cell Counting Kit was used to measure the cell survival rate according to the manufacturer's protocol. Results were shown as mean \pm standard deviation (SD) ($n = 3$).

In vitro MR imaging

AntiGPC3-PBNPs aqueous dispersion at different concentrations were investigated by T1/T2-weighted MRI on a 9.4 T small animal MRI scanner (Bruker Avance II 500WB spectrometer) in order to evaluate their contrast enhancement effect. The T1/T2-weighted imaging was performed by using an inversion recovery gradient echo sequence with TE = 4 ms, a slice thickness of 0.5 mm, a FOV of 3.0×3.0 cm and a matrix size of 128×128 . Afterwards, the contrast enhancement effects of antiGPC3-PBNPs within HepG2 cells were further studied as follows: the HepG2 cells were seeded in 6 well plates (5×10^5 /well) and cultured overnight, then incubated with antiGPC3-PBNPs (1000 ppm) for 12 hours. After washing with PBS buffer for 3 times, the cells were harvested and then embedded into 1 mL 1% (w/v) agarose solution before MRI. The MRI experiments of antiGPC3-PBNPs incubated HepG2 cells were performed under the exactly same parameters as in the in vitro experiments.

Results and discussion

Preparation and Characterization of antiGPC3-PBNPs

The PBNPs were prepared in a simple one-step aqueous solution route by using citric acid as the surface capping agent, which could prevent PBNPs to form aggregation and mediate the size of PBNPs. Then, the targeting modification on the surface of the PBNPs was achieved via a direct single-step EDC/NHS surface coupling method. Compared with the widely used traditional two-step coupling method (refers to firstly activate carboxylate particles with EDC/NHS, and then react with amine-containing molecules) in which the fussy operation and the strict limitations per step have hindered the application for mass production because of its high quality control³¹, here the use of the single-step EDC/NHS method made the whole antiGPC3-PBNPs preparation procedure simple, efficient and stable. The overall experimental design and the synthetic procedure is schematically illustrated in Figure 1.

The typical morphology and the particle size of the antiGPC3-PBNPs were analyzed by the scanning electron microscope (SEM) and the transmission electron microscope (TEM). As shown in Figure 2 and Figure S1†, antiGPC3-PBNPs with an average diameter of 21 nm and 118 nm were both obtained by varying the content of citric acid in the

synthetic procedure. It has been demonstrated that NPs with the a diameter less than 20 nm were very susceptible to renal

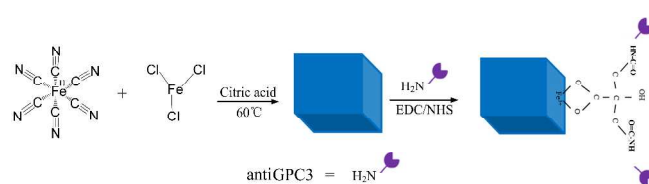


Figure 1. Overview of the synthetic procedure of antiGPC3-PBNPs.

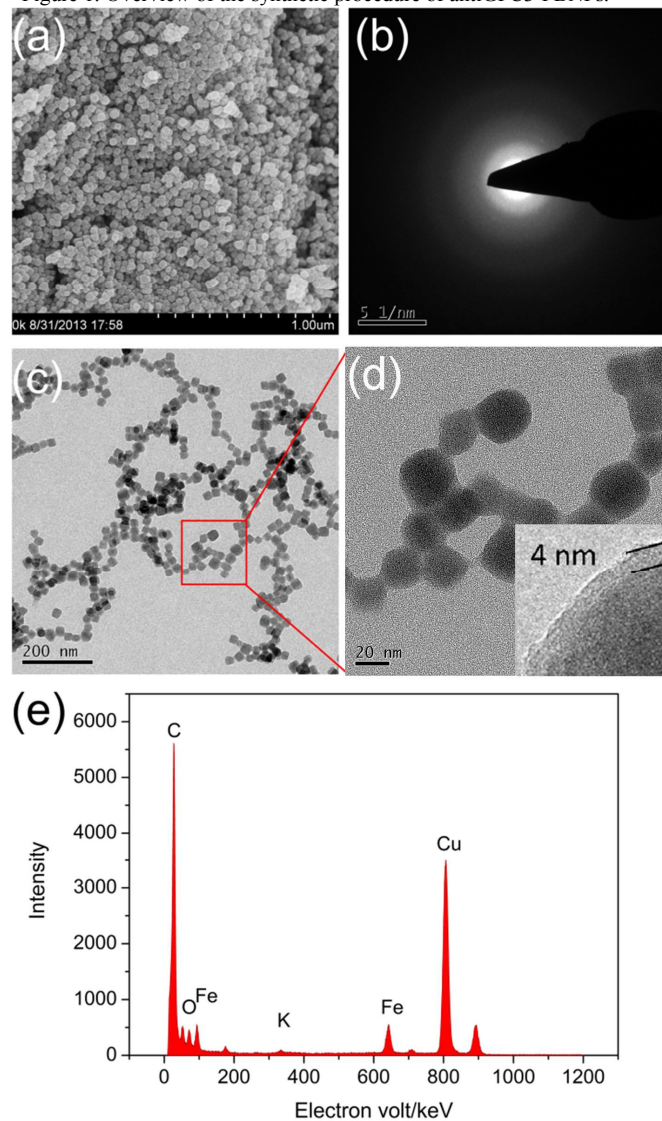


Figure 2. Morphological characterization of the antiGPC3-PBNPs. (a) SEM. (b) SAED pattern. (c) TEM. (d) An enlarged image of TEM, the antiGPC3 coating layer was indicated. (e) EDS analysis.

clearance, but NPs with a diameter larger than 50 nm could be eliminated by the body's reticular endothelial system (RES) or cause a blockage of the blood vessels^{16, 39}. Therefore, to increase the bloodstream circulation time, the optimum intravenously administered NPs should have a diameter

between 20 and 50 nm, which could extravasate from vasculature then enter into the tumor microenvironment via enhanced permeability and retention (EPR) effect and avoid clearance by the RES⁴⁰. Consequently, the ability to maintain the size of the NPs or avoid their aggregation was a key criterion for the use of NPs in biomedical applications³⁹. Based on the above considerations, antiGPC3-PBNPs with an average diameter of 21 nm were selected for the further study. Both the SEM and TEM images (Figure 2a, 2c and 2d) revealed that the antiGPC3-PBNPs were well-formed cubes with a narrow size distribution, and the thickness of antiGPC3 coating layer was 4 nm which was distinguished by the different contrast between the antiGPC3 coating layer and PBNPs (Figure 2d). Dynamic light scattering (DLS) studies revealed the average hydrodynamic size of PBNPs and antiGPC3-PBNPs in water should be 62.2 nm and 100.9 nm according to the scattering intensity, respectively (Figure S4 a and b). The average hydrodynamic size of antiGPC3-PBNPs is larger than that of PBNPs as the antiGPC3-PBNPs coating. However, the hydrodynamic size of antiGPC3-PBNPs and antiGPC3 are both larger than their diameter determined by TEM, this might be because of small aggregations of a few nanoparticles obtained from water phase synthesis; this phenomenon also has been reported by other literatures^{41,42}. The poly-dispersity index (PDI) was measured to be 0.167, which was indicating a relatively good disperse distribution. The zeta potential of antiGPC3-PBNPs (ζ) was ca. -21.3 mV (Figure S4 d). Several well-defined diffraction rings were observed in the typical selected area electron diffraction (SAED) pattern of antiGPC3-PBNPs (Figure 2b), which demonstrated that the nanoparticles exhibited a single-crystal-like feature²⁴. The presence of iron element in the antiGPC3-PBNPs was confirmed by Energy dispersive spectroscopy (EDS) analysis (Figure 2e).

The unbounded GPC3 antibody in the supernatants was determined to be 10.48 μg by using the Enhanced BCA Protein Assay Kit according to the manufacturer's protocol. Therefore, the bounding content of GPC3 antibody was 29.52 $\mu\text{g}/\text{mg}$ PBNPs, which means the coupling efficiency was 73.8%. Namely, it can be calculated that each PB nanoparticle could bind three GPC3 antibodies by theoretical calculation based on the average size of antiGPC3-PBNPs.

The Vis-NIR absorption spectra of antiGPC3-PBNPs were analyzed by using a TU-1950 UV-Vis spectrophotometer. As shown in Figure 3a, both the PBNPs and the antiGPC3-PBNPs displayed a broad absorption band from 500 nm to 900 nm with a maximum absorption peak at 715 nm in the NIR region, which was attributed to the charge transfer transition between Fe(II) and Fe(III) in the PBNPs²². Strong absorption in the NIR region (700~900 nm) could still be observed after the antibody-coupling reaction, which was essential for the NIR laser driven photo-thermal applications. Furthermore, the antiGPC3-PBNPs were dispersed very well in DMEM culture medium supplemented with 10% fetal bovine serum (FBS), without any macroscopic aggregates, as evidenced by the linearly increased absorbance with the increasing of antiGPC3-PBNPs concentration in the buffer (Figure 3b and 3c), as well as the

DLS results shown in Figure 3d, which was clearly demonstrated that the antiGPC3-PBNPs maintained its hydrodynamic size around 100 nm in DMEM with 10% FBS (Figure 3d).

Temperature elevation induced by NIR laser irradiation

The strong absorption of antiGPC3-PBNPs in the NIR region could contribute to the NIR laser-induced thermal effect, which could be used for PTT therapy. The photo-thermal effect induced by NIR laser irradiation (808 nm, 2 W/cm²) was investigated by monitoring the temperature of 1.0 mL antiGPC3-PBNPs with various concentrations (0, 45.5, 90.9 ppm). As shown in Figure 4a, after exposure at the NIR laser light for 10 min, the temperature of antiGPC3-PBNPs dispersions with the concentration of 45.5 ppm and 90.9 ppm increased from 31.9°C to 51.6°C, 30.8°C to 69.5°C, respectively. As for 90.9 ppm concentration, the temperature was increased to above 60°C after the irradiation. Even after irradiation for a short time less than 1 min, the temperature then could reach to the critical temperature (43°C) which is sufficient to kill cancer cells⁴³. In comparison, the temperature of DI water without antiGPC3-PBNPs showed no significant changes when exposed to the laser. Heating up to 43°C or above in tumor by the antiGPC3-PBNPs would be easily achieved as the normal body temperature is already 36.2~37.5°C. These results suggested that the antiGPC3-PBNPs also could rapidly and efficiently convert the 808 nm laser energy into thermal energy after coupling GPC3 antibodies to the surface of PBNPs. Moreover, the photo-thermal stability of the antiGPC3-PBNPs was also studied (Figure 4b). The temperature cycling of antiGPC3-PBNPs dispersions during 3 rounds of repeated irradiation indicated that the antiGPC3-PBNPs had excellent photo-thermal stability. The observed photo-thermal stability probably due to following reasons: Firstly, the strong NIR absorption of PBNPs is attributed to the charge transfer transition between Fe (2+) and Fe (3+)^{22, 44, 45}; it means that the Fe (2+) loses an electron to become Fe (3+), and the Fe (3+) receives an electron to become Fe (2+); meanwhile, it also has been reported that the chemical bonds of Fe²⁺—CN—Fe³⁺ were strong enough to suffer the electron transfer, and would not be broken by this process^{24, 25}; in such case, the molecular structure basis of PBNPs actually does not change at all, and the charge transfer transition can re-happen again following another round of laser irradiation; therefore, the NIR absorption of PBNPs would not be affected by cyclic laser irradiation at all, which means the photo-thermal stability will not be affected. Secondly, the PBNPs were not destroyed by the cyclic irradiation, which is based on the evidence of no apparently particle size change. As shown in Fig. 3d, the size of antiGPC3-PBNPs was not apparently changed during 3 rounds of repeated irradiation with the 808 nm NIR laser. These results implied the antiGPC3-PBNPs could reuse for several times during practical applications. The above data demonstrated that antiGPC3-PBNPs could be

employed as an efficient NIR-light absorber for photo-thermal tumor therapy.

Photo-thermal cytotoxicity of antiGPC3-PBNPs

To evaluate the localized tumor photo-thermal effect of antiGPC3-PBNPs, HepG2 cells were cultured in six-well plate then incubated with 50 ppm antiGPC3-PBNPs, afterwards irradiated with an NIR laser (808 nm, 2 W) for 10 min. Fluorescence staining by the live cell permeable dye calcein AM was carried out for visualization of living cells. As shown in Figure 5d, HepG2 cells treated with antiGPC3-PBNPs plus a 10 min NIR laser irradiation caused a remarkable cell death. Most of the cells outside of the illumination zone exhibited the green fluorescence of calcein, indicating the survival of HepG2 cells, while a small part of cells close to the outside edge of the illumination zone also died because of the spreading of heat outside to the laser irradiation area. Nevertheless, comparing to the negative control without both antiGPC3-PBNPs and laser irradiation (Figure 5a), no apparent cell death was observed in cells treated with antiGPC3-PBNPs alone or with laser

irradiation alone (Figure 5b and 5c). These results suggested that antiGPC3-PBNPs could specific mediate the photo-thermal destruction of HepG2 cells. We further evaluated the photo-thermal cytotoxicity of antiGPC3-PBNPs with and without laser irradiation on HepG2 cells using a Cell Counting Kit-8 (CCK-8) assay. HepG2 cells were incubated with gradient concentrations of antiGPC3-PBNPs for 4 hours. As shown in Figure 5e, in the presence of laser irradiation for 8 minutes, the cell viabilities of HepG2 cells significantly decreased with the increasing concentration of antiGPC3-PBNPs from 0 ppm to 20 ppm. There are less than 10% of HepG2 cells remaining viable at the concentration of 15 ppm. In contrast, HepG2 cells treated with antiGPC3-PBNPs without laser irradiation remained more than 90% viable even at a high dose (20 ppm), which suggested that antiGPC3-PBNPs itself had low toxicity to HepG2 cells. These experimental findings demonstrated that the combination of antiGPC3-PBNPs and NIR laser illumination could locally kill the liver tumor cells in vitro, indicating a significant photo-thermal therapeutic effect of the antiGPC3-PBNPs, and clearly revealed that the antiGPC3-PBNPs could act as a potential NIR photo-absorber for PTT treatment of HCC.

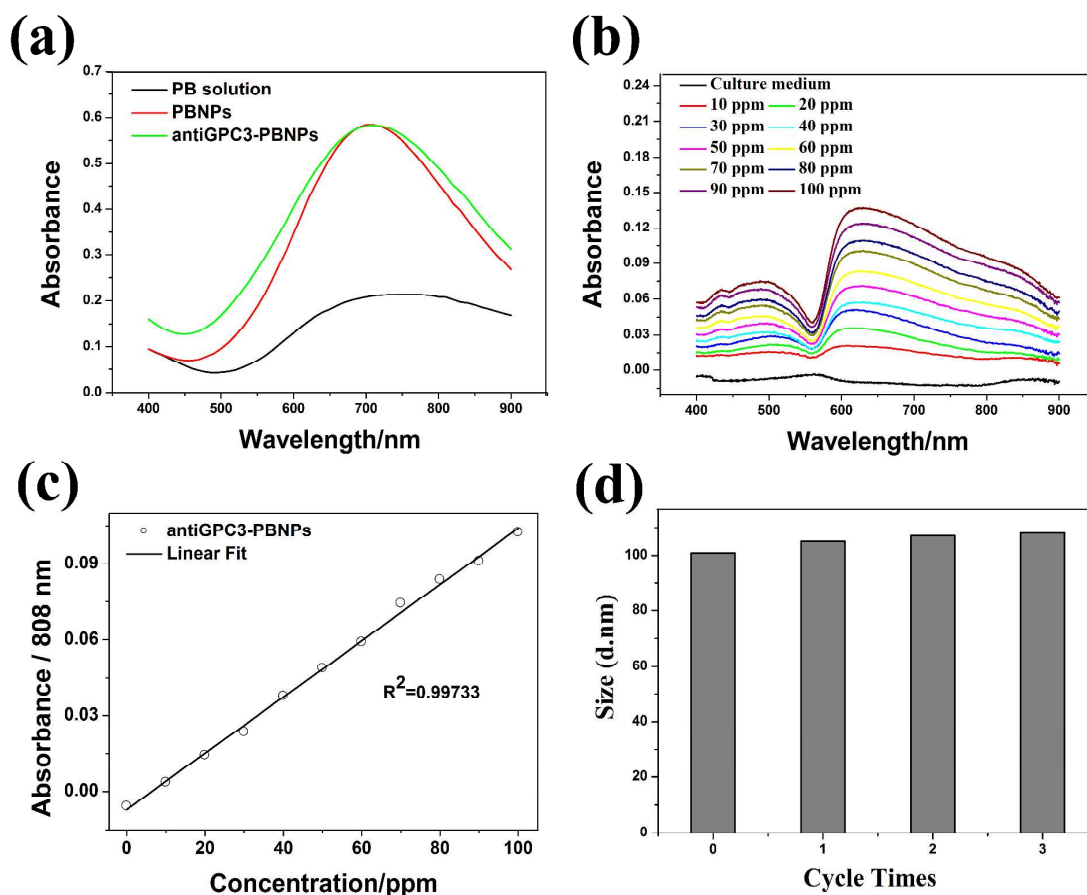


Figure 3. (a) Vis-NIR absorption spectra of the PB solution, PBNPs and antiGPC3-PBNPs with the same Fe concentration in water (50 ppm); (b) Vis-NIR absorption spectra of antiGPC3-PBNPs with different concentrations in the DMEM culture medium containing 10% FBS; (c) Fitting curve of UV absorption values of the antiGPC3-PBNPs in DMEM culture medium containing 10% FBS at 808 nm with different concentrations; (d) The average hydrodynamic size of antiGPC3-PBNPs over 3 rounds of "Laser turn on/off" cycling with the 808 nm NIR laser irradiation.

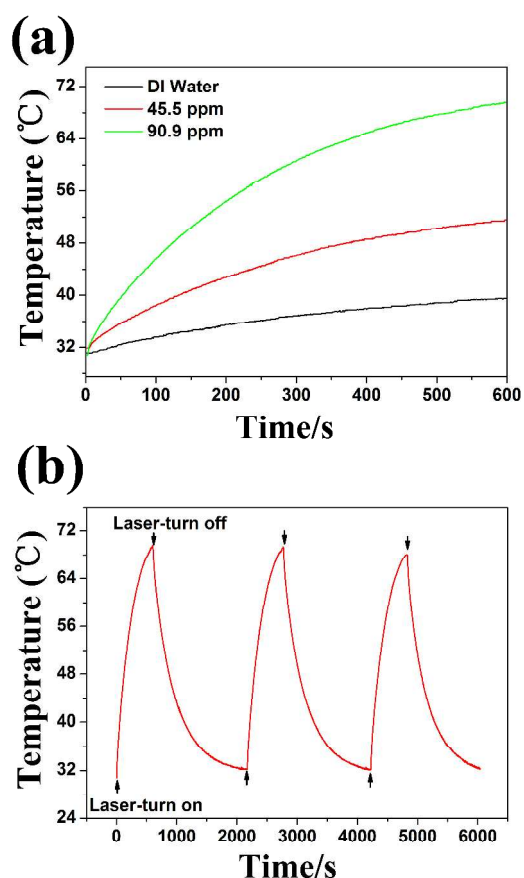


Figure 4. (a) Temperature elevation of antiGPC3-PBNPs after exposure to NIR laser (808 nm, 2 W/cm^2) for 10 min. DI water was used as a control. (b) Temperature elevation of antiGPC3-PBNPs (90.9 ppm) over 3 rounds of "Laser turn on/off" cycling with the 808 nm NIR laser.

Non-toxicity or low toxicity is a key criterion for biomedical applications of any nanoparticles⁴⁶. A further evaluation of cytotoxicity to normal hepatocytes of the antiGPC3-PBNPs in the absence of laser irradiation was also carried out by performing CCK-8 assay. The normal HL-7702 cells were incubated with gradient concentrations (0, 25, 50, 100, 150, 200, 400 ppm) of antiGPC3-PBNPs solution 24 h and 48 h, respectively. It was found that the percentages of viable HL-7702 cells, which are exposed to antiGPC3-PBNPs with the concentration as high as 400 ppm for both 24 h and 48 h, were even more than 80% (Figure 5f), which suggested that the prepared antiGPC3-PBNPs have a very good biocompatibility.

Confocal fluorescence microscopy studies of the cellular uptake efficiency

To investigate the cellular uptake and localization of the antiGPC3-PBNPs in HepG2 cells, FITC was used to label antiGPC3-PBNPs and the fluorescence emission spectrum of FITC-antiGPC3-PBNPs was shown in Figure S2†. Then HepG2 cells, HeLa cells and normal HL-7702 cells were incubated with the prepared FITC-labeled antiGPC3-PBNPs. The confocal fluorescence image was visualized by CLSFM

with a 488 nm excitation. Figures 6 showed that the FITC-labeled antiGPC3-PBNPs (green color emitted) were gradually internalized after incubated with HepG2 cells for 2-h and 4-h durations. To determine the sub-cellular localization of NPs, we added the bright field images to overlay with DAPI and FITC channel in Figure 6. Based on these merged image, we can confirm that some of the antiGPC3-PBNPs appeared to attach to the cell surface after 2hrs incubation; the green fluorescent signal was significantly increased in the peri-nuclear regions after 4hrs incubation (Figure 6b and 6c), which clearly demonstrated the internalization of the antiGPC3-PBNPs. As shown in Figure 6d, we have significantly reduced antiGPC3-PBNPs internalization when the free antiGPC3 antibody along with the antiGPC3-PBNPs were incubated with the HepG2 cells together, might due to the less binding of antiGPC3-PBNPs resulting from the free antiGPC3 antibody competition.

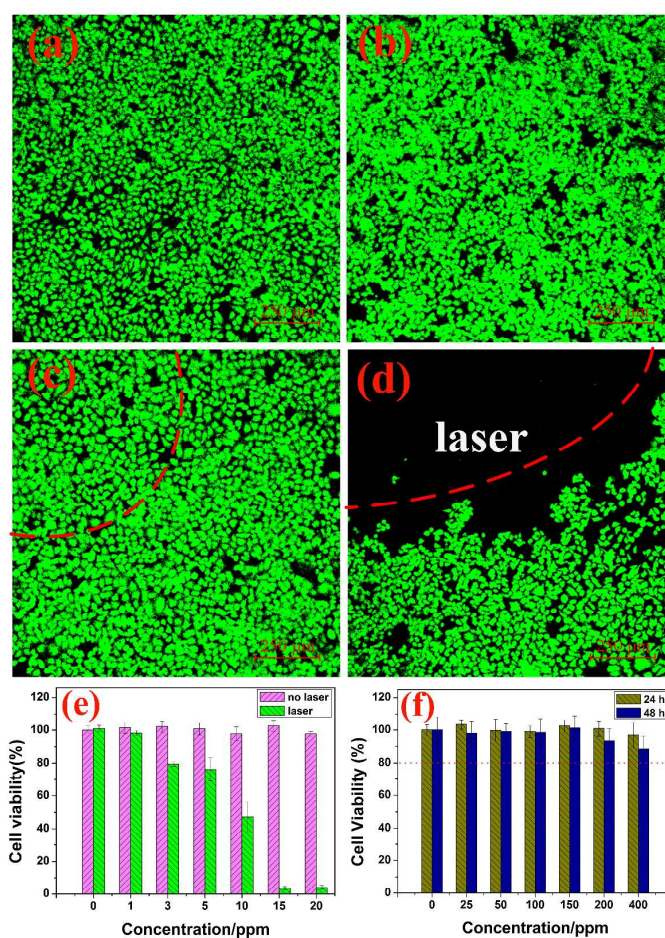


Figure 5. Photo-thermal cancer cell killing efficacy of antiGPC3-PBNPs. (a) without both antiGPC3-PBNPs and laser irradiation; (b) 50 ppm antiGPC3-PBNPs but without laser irradiation; (c) without NPs but with laser irradiation; (d) 50 ppm antiGPC3-PBNPs with 10min laser irradiation. Scale bar: $250 \mu\text{m}$; (e) Cell viabilities of HepG2 cells treated with different dosages of antiGPC3-PBNPs with or without the laser irradiation for 8 min; (f) Cell viabilities of normal HL-7702 cells with 24 or 48 hours exposure to various concentrations of antiGPC3-PBNPs but without laser irradiation.

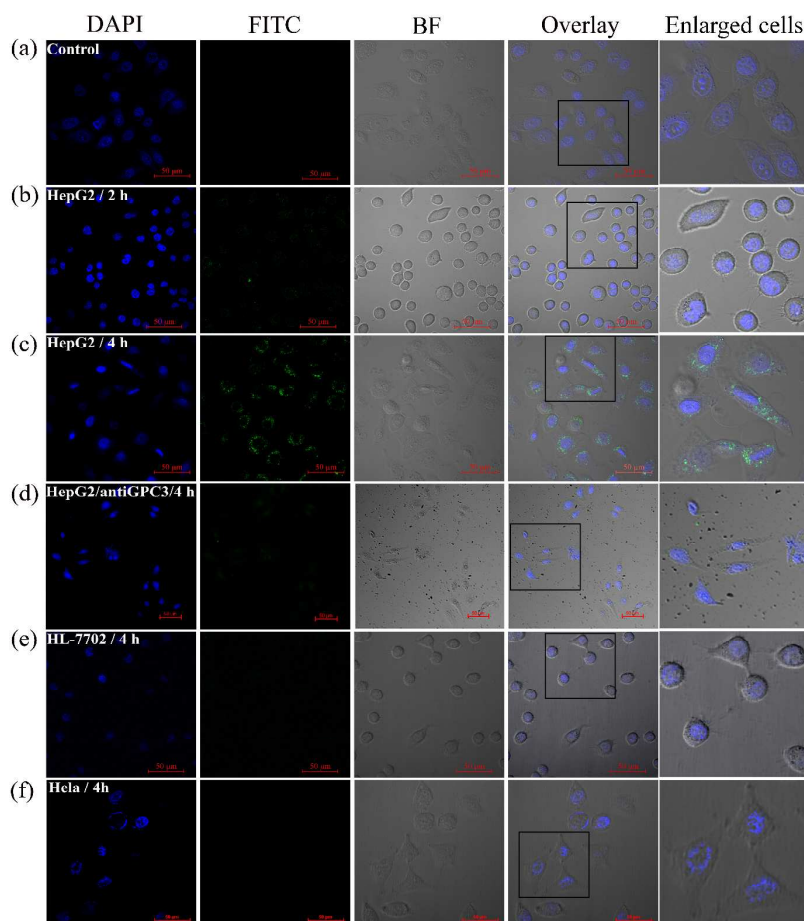


Figure 6. Confocal fluorescence images of cells incubated with 250 ppm FITC-labeled antiGPC3-PBNPs in DMEM medium. (a) HepG2 cells only. HepG2 cells incubated with FITC-labeled antiGPC3-PBNPs for (b) 2 hours and (c) 4 hours. (d) Competition assays for cellular uptake of FITC-labeled antiGPC3-PBNPs in HepG2 cells. (e) (f) the control studies by using normal HL-7702 cells and HeLa cells (4-h incubation). Nuclei were counter stained blue with DAPI. Scale bar: 50 μm .

These observations indicated that the amount of antiGPC3-PBNPs taken up by HepG2 cells was significantly higher due to the receptor mediated endocytosis. These results implied that antiGPC3-PBNPs could retain their GPC3 binding activity and specificity, meanwhile, it was confirmed that the nanoprobe could specifically and effectively target GPC3-positive liver tumor cells rather than other none specific cancer cell types.

Quantification of antiGPC3-PBNPs uptake by ICP-MS

The increased cellular uptake of antiGPC3-PBNPs by HepG2 cells was further confirmed through the quantification of dose-dependent and time-dependent uptake by HepG2 cells, which was analyzed by ICP-MS. As shown in Figure 7, the iron contents in HepG2 and HL-7702 cells were measured by ICP-MS and the results demonstrated that antiGPC3-PBNPs were internalized by HepG2 and HL-7702 cells in a concentration-dependent and time-dependent manner.

Figure 7a showed that both the intracellular iron content in HepG2 and HL-7702 cells were increased with the increasing

of antiGPC3-PBNPs concentrations. A further two-fold increase of antiGPC3-PBNPs incorporated into HepG2 cells was observed at the concentration of 250 ppm compared to the concentration of 50 ppm. Moreover, the uptake of antiGPC3-PBNPs by HepG2 cells was significantly higher than that by HL-7702 cells at all concentrations ($P < 0.05$). Especially at the 250 ppm concentration of antiGPC3-PBNPs, the iron content in HepG2 cells was almost twice higher than that in HL-7702 cells. The amounts of iron incorporated into HepG2 cells were also significantly different between the antiGPC3-PBNPs and PBNPs. However, as a control, the amounts of PBNPs internalized by HepG2 and HL-7702 cells showed no significant difference.

As shown in Figure 7b, the time dependent cellular uptake (1, 2 and 4 h) of a constant concentration (250 ppm) of antiGPC3-PBNPs was studied. It showed that the incorporation of antiGPC3-PBNPs or PBNPs by HepG2 and HL-7702 cells increased along with the incubation time. When compared with the amount of the iron content in HepG2 cells incubated with antiGPC3-PBNPs for 1 hour, the iron content of 2h incubation

time had a more than twice increase. Especially, within an equal incubation time, the amount of iron incorporation into HepG2 cells incubated with antiGPC3-PBNPs was significantly higher than HepG2 cells incubated with PBNPs, and HL-7702 cells incubated with antiGPC3-PBNPs or PBNPs.

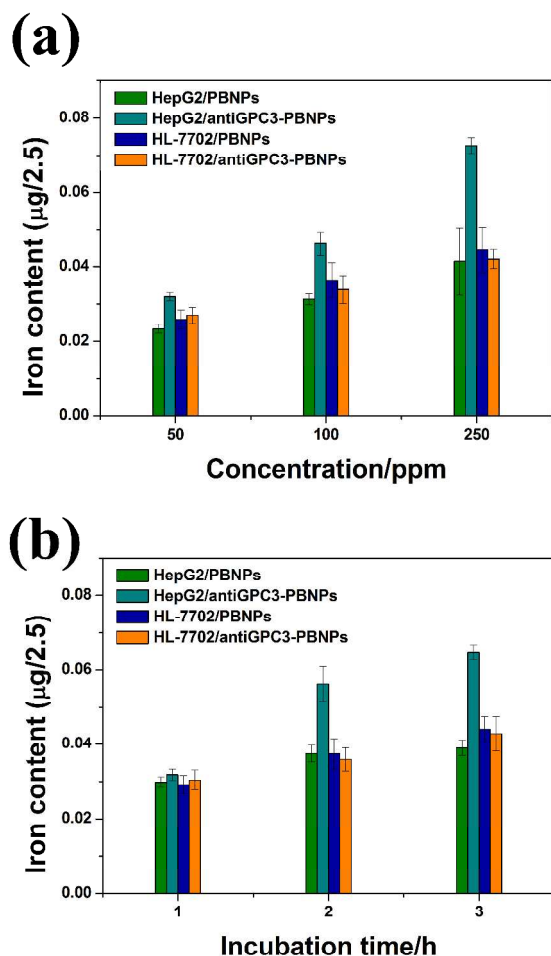


Figure 7. The iron content uptakes by HepG2 cells or HL-7702 (a) in a dose-dependent manner and (b) in a time-dependent manner.

These experimental data indicated that antiGPC3-PBNPs could be taken up more efficiently in a specific receptor mediated manner by HepG2 cells, while the PBNPs itself exhibited low non-specific uptake or binding by both HepG2 and HL-7702 cells. Thus, the combination of confocal microscopy studies and quantification of iron content by ICP-MS conclusively proved the significantly increased GPC3 antibody-mediated cellular uptake of the antiGPC3-PBNPs by HepG2 cells.

In vitro MR imaging

Various concentrations of antiGPC3-PBNPs dispersed in DI water were used to perform the proton T_1 and T_2 relaxation measurements, as well as the phantom imaging by using a 9.4 T MRI system to investigate the potential use of antiGPC3-

PBNPs as a MRI contrast agent for HCC imaging. The T_1 and T_2 relaxation time for each sample at 20°C was shown in Table 1 and the results indicated that the nanoparticles could shorten both the T_1 and T_2 relaxation time. Further analysis of the observed rates of both longitudinal and transversal relaxation revealed a linear dependence on the concentration of dispersed antiGPC3-PBNPs in all the measurements (Figure S3†). The longitudinal and transverse co-efficient relaxivity values, r_1 and r_2 , which were both determined from the slope of the plot of $1/T_1$ and $1/T_2$ versus the sample concentration, were $0.14 \text{ mM}^{-1}\text{s}^{-1}$ and $11.73 \text{ mM}^{-1}\text{s}^{-1}$, respectively. Furthermore, the ability to enhance the contrast in MRI images was evaluated by acquiring the T_1 -weighted and T_2 -weighted MR phantom imaging slices of antiGPC3-PBNPs suspensions in DI water with various concentrations. As shown in Figure 8a, the T_1 images became progressively brighter along with the increasing of antiGPC3-PBNPs concentration, which was contrary to the change of the T_2 images, and thus indicated the incremental signal intensity at increased antiGPC3-PBNPs concentrations in the range from 50 to 300 ppm.

We next used antiGPC3-PBNPs for MR imaging of cancer cells. The HepG2 cells incubated with the antiGPC3-PBNPs showed significantly reduced signal in the T_2 -weighted MR images in comparison to the untreated cells, which is consistent with the in vitro experiments. However, the contrast of T_1 -weighted MR images were not significantly enhanced, it might due to the less nanoparticles presented inside the cells comparing to the pure solution. These results indicated that the antiGPC3-PBNPs would be a promising candidate as a contrast agent for HCC MR imaging, because of the excellent T_2 -weighted MRI contrast enhancing (Figure 8b).

Table 1. The results of T_1 and T_2 time values of antiGPC3-PBNPs dispersions at various concentrations.

	H ₂ O	10 ppm	50 ppm	100 ppm	300 ppm
T_1 time (ms)	2600.93 ±19.32	2593.12 ±18.74	2580.07 ±19.86	2327.77 ±50.25	1657.48 ±15.94
T_2 time (ms)	601.51 ±14.89	597.72 ±11.15	380.01 ±7.37	151.25 ±3.51	47.74 ±0.94

Table 2. The results of T_1 and T_2 time values of antiGPC3-PBNPs uptake by HepG2 cells.

	Cell only	1000 ppm
T_1 time (ms)	2679.38 ±17.13	2856.62 ±16.75
T_2 time (ms)	104.845 ±2.62	90.2884 ±1.95

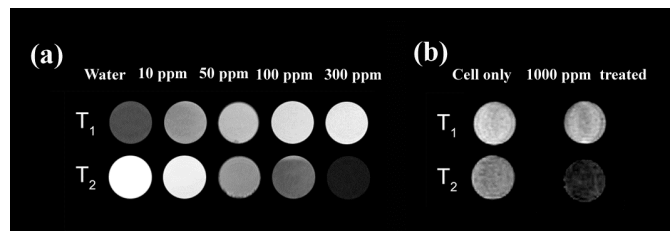


Figure 8. (a) T_1 and T_2 weighted MR images of antiGPC3-PBNPs in aqueous solution at the concentration of 10, 50, 100 and 300 ppm respectively; (b) T_1 and T_2 weighted MR images of HepG2 cells incubated with antiGPC3-PBNPs.

Conclusions

In summary, we have reported a simple synthesis strategy for the fabrication of GPC3 monoclonal antibody functionalized PBNPs by using the ENC/NHS coupling method. The antiGPC3-PBNPs were applied as a multi-functional nanoprobe for the targeted MR imaging and photo-thermal destruction of hepatocellular carcinoma. Several characterization methods such as SEM, TEM and Vis-NIR absorption spectra were used to investigate the physical properties of the multifunctional nanoparticles. The results showed that antiGPC3-PBNPs exhibited a favorable dispersity and good stability. Meanwhile, the targeting cellular uptake experiments showed a significantly increased antibody-mediated active targeting efficiency for liver tumor cells. Moreover, in the presence of antiGPC3-PBNPs, significant photo-thermal cytotoxicity and obvious MR imaging enhancements were obtained, which suggested the effective hyper-thermal therapeutic functions and the excellent MRI contrast-enhancing ability. Hence, in view of the advantages mentioned above as well as the excellent biocompatibility, we envision that the described antiGPC3-PBNPs could be used as a promising nanoprobe for further treating and early diagnosis of hepatocellular carcinoma.

Acknowledgements

This work is supported by the key project of National Science and technology of China (Grant No. 2012ZX10002010-001-006, and Grant No. 2012ZX10002016-013), the National Natural Science Foundation of China (Grant No. 31201008), the key project of Science and Technology Department of Fujian Province (Grant No. 2011Y0022), the Natural Science Foundation of Fujian Province (Grant No. 2011J01162), the University Foundation of Fujian Province (Grant No. JK2011021), the University Natural Science Foundation of Jiangsu Province (Grant No. 12KJB180013), the Scientific Foundation of Fuzhou Health Department (Grant No. 2013-S-wq17), and the Research Development Foundation of Fujian Medical University (Grant No. FZS13001Y, and Grant No. FZS13005Z).

Notes

1. Mengchao Hepatobiliary Hospital of Fujian Medical University, Fuzhou 350025, P. R. China.
2. The Liver Center of Fujian Province, Fujian Medical University, Fuzhou 350025, P. R. China.
3. Liver Disease Center, The First Affiliated Hospital of Fujian Medical University, Fuzhou 350007, P. R. China.
4. Department of Pathology, School of Basic Medical Science, Fujian Medical University, Fuzhou 350004, P. R. China.
5. The Key Lab of Analysis and Detection Technology for Food Safety of the MOE, College of Chemistry, Fuzhou University, Fuzhou 350002, P.R. China.

*Corresponding author (correspondence should be addressed to X. Liu and JF. Liu), # Equal Contribution Authorship.

E-mail address: xiaoloong.liu@gmail.com (X. Liu),

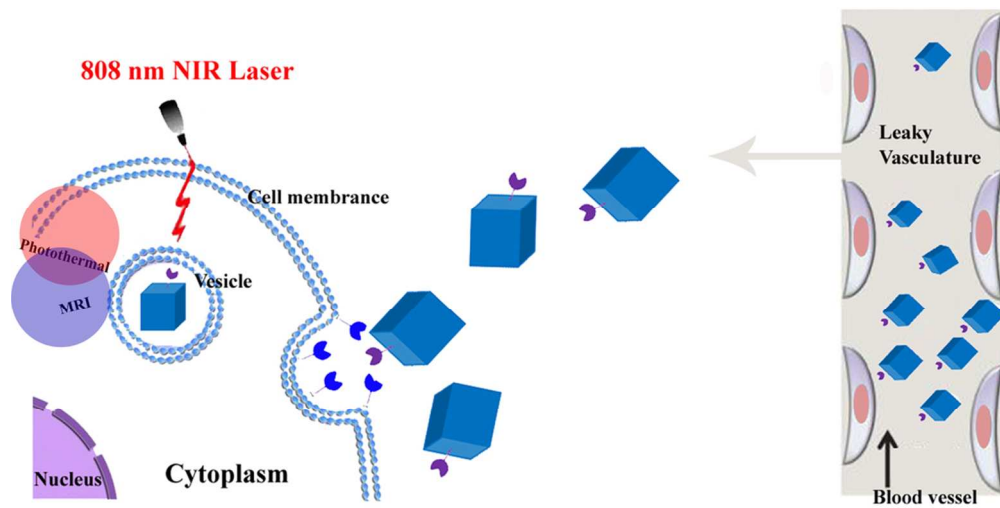
drjingfeng@126.com (JF. Liu)

†Electronic Supplementary Information (ESI) available: Supporting figures. See DOI: 10.1039/b000000x/

References

1. X. B. Man, L. Tang, B. H. Zhang, S. J. Li, X. H. Qiu, M. C. Wu and H. Y. Wang, *Liver International*, 2005, **25**, 962-966.
2. M. Sherman, in *Seminars in liver disease*, © Thieme Medical Publishers, 2010, pp. 003-016.
3. P. Ferenci, M. Fried, D. Labrecque, J. Bruix, M. Sherman, G. Lau, F. Carillo, J. Krabshuis and A. Le Mair, *J Gastrointest Liver Dis*, 2010, **19**, 311-317.
4. Y.-H. Tang, T.-F. Wen and X. Chen, *Hepato-gastroenterology*, 2012, **59**, 1393-1397.
5. E. Melloul, M. Lesurtel, B. I. Carr and P.-A. Clavien, in *Seminars in oncology*, Elsevier, 2012, pp. 510-521.
6. Y.-C. Shen, C. Hsu, C.-C. Cheng, F.-C. Hu and A.-L. Cheng, *Oncology*, 2012, **82**, 275-289.
7. I. E. El Mehdi Tazi, H. M'rabti, A. Touyar and P. H. Errihani, *North American journal of medical sciences*, 2011, **3**, 167.
8. J. Bruix and J. M. Llovet, *The Lancet*, 2009, **373**, 614-616.
9. N. N. Massarweh, J. O. Park, F. Farjah, R. S. Yeung, R. G. Symons, T. L. Vaughan, L.-M. Baldwin and D. R. Flum, *Journal of the American College of Surgeons*, 2010, **210**, 441-448.
10. J. Bruix and M. Sherman, *Hepatology*, 2005, **42**, 1208-1236.
11. Z. Zhang, L. Wang, J. Wang, X. Jiang, X. Li, Z. Hu, Y. Ji, X. Wu and C. Chen, *Advanced Materials*, 2012, **24**, 1418-1423.
12. H. Park, J. Yang, J. Lee, S. Haam, I.-H. Choi and K.-H. Yoo, *ACS nano*, 2009, **3**, 2919-2926.
13. J. R. Whitney, S. Sarkar, J. Zhang, T. Do, T. Young, M. K. Manson, T. A. Campbell, A. A. Puretzky, C. M. Rouleau and K. L. More, *Lasers in surgery and medicine*, 2011, **43**, 43-51.
14. Q. Tian, M. Tang, Y. Sun, R. Zou, Z. Chen, M. Zhu, S. Yang, J. Wang, J. Wang and J. Hu, *Advanced Materials*, 2011, **23**, 3542-3547.
15. V. U. Fiedler, H. J. Schwarzmaier, F. Eickmeyer, F. P. Müller, C. Schoepf and P. R. Verreet, *Journal of Magnetic Resonance Imaging*, 2001, **13**, 729-737.
16. Z. Zha, X. Yue, Q. Ren and Z. Dai, *Advanced Materials*, 2012.

17. J. Shah, S. Park, S. Aglyamov, T. Larson, L. Ma, K. Sokolov, K. Johnston, T. Milner and S. Y. Emelianov, *Journal of biomedical optics*, 2008, **13**, 034024-034024-034029.
18. L. R. Hirsch, R. J. Stafford, J. A. Bankson, S. R. Sershen, B. Rivera, R. E. Price, J. D. Hazle, N. J. Halas and J. L. West, *Proceedings of The National Academy of Sciences of The United States of America*, 2003, **100**, 13549-13554.
19. M. Kangasniemi, R. J. McNichols, J. A. Bankson, A. Gowda, R. E. Price and J. D. Hazle, *Lasers in surgery and medicine*, 2004, **35**, 41-50.
20. S.-W. Chou, Y.-H. Shau, P.-C. Wu, Y.-S. Yang, D.-B. Shieh and C.-C. Chen, *Journal of the American Chemical Society*, 2010, **132**, 13270-13278.
21. V. Rieke and K. Butts Pauly, *Journal of Magnetic Resonance Imaging*, 2008, **27**, 376-390.
22. G. L. Fu, W. Liu, S. Feng and X. Yue, *Chemical Communications*, 2012, **48**, 11567-11569.
23. S. Zhang, Z. Zha, X. Yue, X. Liang and Z. Dai, *Chemical Communications*, 2013, **49**, 6776-6778.
24. M. Shokouhimehr, E. S. Soehnlén, J. Hao, M. Griswold, C. Flask, X. Fan, J. P. Babilion, S. Basu and S. D. Huang, *Journal of Materials Chemistry*, 2010, **20**, 5251-5259.
25. M. Shokouhimehr, E. S. Soehnlén, A. Khitrin, S. Basu and S. D. Huang, *Inorganic Chemistry Communications*, 2010, **13**, 58-61.
26. F. Jia, X. Zhang, Y. Xu and Z. Meng, *Nan fang yi ke da xue xue bao = Journal of Southern Medical University*, 2009, **29**, 191.
27. C. M. Lee, H. J. Jeong, E. M. Kim, D. W. Kim, S. T. Lim, H. T. Kim, I. K. Park, Y. Y. Jeong, J. W. Kim and M. H. Sohn, *Magnetic Resonance in Medicine*, 2009, **62**, 1440-1446.
28. T. Huo, X. Du, S. Zhang, X. Liu and X. Li, *European journal of radiology*, 2010, **73**, 420-427.
29. S. G. Crich, S. Lanzardo, D. Alberti, S. Belfiore, A. Ciampa, G. B. Giovenzana, C. Lovazzano, R. Pagliarin and S. Aime, *Neoplasia (New York, NY)*, 2007, **9**, 1046.
30. M. L. Schipper, G. Iyer, A. L. Koh, Z. Cheng, Y. Ebenstein, A. Aharoni, S. Keren, L. A. Bentolila, J. Li and J. Rao, *Small*, 2009, **5**, 126-134.
31. H. Lee, E. Lee, D. K. Kim, N. K. Jang, Y. Y. Jeong and S. Jon, *Journal of the American Chemical Society*, 2006, **128**, 7383-7389.
32. G. Pilia, R. M. Hughes-Benzie, A. MacKenzie, P. Baybayan, E. Y. Chen, R. Huber, G. Neri, A. Cao, A. Forabosco and D. Schlessinger, *Nature genetics*, 1996, **12**, 241-247.
33. Y. Li, Z. Chen, F. Li, J. Wang and Z. Zhang, *International journal of nanomedicine*, 2012, **7**, 4593.
34. J. O. Park, Z. Stephen, C. Sun, O. Veiseh, F. M. Kievit, C. Fang, M. Leung, H. Mok and M. Zhang, *Molecular imaging*, 2011, **10**, 69.
35. L.-D. Chen, J. Liu, X.-F. Yu, M. He, X.-F. Pei, Z.-Y. Tang, Q.-Q. Wang, D.-W. Pang and Y. Li, *Biomaterials*, 2008, **29**, 4170-4176.
36. S.-J. Wang, C.-S. Chen and L.-C. Chen, *Science and Technology of Advanced Materials*, 2013, **14**, 044405.
37. L. Zhao, J.-M. Lin and Z. Li, *Analytica chimica acta*, 2005, **541**, 197-205.
38. X. Wang, Q.-Y. Zhang, Z.-J. Li, X.-T. Ying and J.-M. Lin, *Clinica Chimica Acta*, 2008, **393**, 90-94.
39. T. Neuberger, B. Schöpf, H. Hofmann, M. Hofmann and B. von Rechenberg, *Journal of Magnetism and Magnetic Materials*, 2005, **293**, 483-496.
40. H. S. Choi, W. Liu, P. Misra, E. Tanaka, J. P. Zimmer, B. I. Ipe, M. G. Bawendi and J. V. Frangioni, *Nature biotechnology*, 2007, **25**, 1165-1170.
41. K. Andreas, R. Georgieva, M. Ladwig, S. Mueller, M. Notter, M. Sittlinger and J. Ringe, *Biomaterials*, 2012, **33**, 4515-4525.
42. R. Hachani, M. Lowdell, M. Birchall and N. T. K. Thanh, *Nanoscale*, 2013, **5**, 11362-11373.
43. H. GM, *Proc Natl Acad Sci USA*, 1975, **72**, 937-940.
44. S. Vaucher, M. Li and S. Mann, *Angewandte Chemie International Edition*, 2000, **39**, 1793-1796.
45. J. F. Zhai, Y. M. Zhai, D. Wen and S. J. Dong, *Electroanalysis*, 2009, **21**, 2207-2212.
46. Y. Liu, K. Ai, J. Liu, Q. Yuan, Y. He and L. Lu, *Angewandte Chemie International Edition*, 2012, **51**, 1437-1442.



50x25mm (600 x 600 DPI)